



## Original article

# Evaluation of the effectiveness of coatings for the protection of outdoor terracotta artworks through artificial ageing tests



S. Spadavecchia<sup>a</sup>, C. Chiavari<sup>a,\*</sup>, F. Ospitali<sup>b</sup>, S. Gualtieri<sup>c</sup>, A.C. Hillar<sup>a</sup>, E. Bernardi<sup>b</sup>

<sup>a</sup> Dept. Cultural Heritage, University of Bologna, via degli Ariani 1, Ravenna, Italy

<sup>b</sup> Dept. Industrial Chemistry "Toso Montanari", University of Bologna, Via Piero Gobetti 85, Bologna, Italy

<sup>c</sup> CNR-ISSMC Istituto di Scienza, Tecnologia e Sostenibilità per lo Sviluppo dei Materiali Ceramici, via Granarolo, 64, Faenza, Italy

## ARTICLE INFO

## Article history:

Received 19 December 2023

Accepted 17 September 2024

## Keywords:

Ceramics

Protective products

Silica nano-coatings

Fluorinated coatings

Artificial ageing

Natural weathering

## ABSTRACT

Historical-artistic heritage, when located outdoor, is heavily targeted by deterioration phenomena such as weathering and air pollution. This is especially true for terracotta artefacts, as the medium porosity which characterizes them makes their damaging easier. Nevertheless, there is limited academic research on conservation strategies with regards to coatings. Consequently, the restoration of the carbonate terracotta sculpture known as "Muro del vento" (Wind Wall) by Domenico Matteucci has become the starting point for an experimental investigation carried out in order to evaluate the effectiveness and durability - for outdoor terracotta artworks - of an array of protective coatings. In this paper, four commercial protective coatings, recommended both for natural and artificial stones, were evaluated: a vinylidene-fluoride-hexafluoropropene copolymer at 3 % in acetone, an aqueous emulsion of alkylpolysiloxane, an aqueous dispersion of functionalized silica nanoparticles, and a nanostructured and functionalized silica gel in hydroalcoholic solution. Coated and uncoated representative calcium-rich terracotta specimens were subjected to two different accelerated ageing procedures: rain runoff test and climatic chamber exposure. Concurrently, a long-term outdoor exposure was set up.

The characterization of the specimens and the evaluation of the coating's performances were carried out through color, contact angles, water absorption and mass variation measurements, 3D digital microscopy, scanning electron microscopy, X-Ray diffraction, Raman micro-Spectroscopy and atomic absorption spectroscopy in order to quantify calcium release in rain.

Overall, the proposed accelerated ageing procedures proved to be successful for evaluating effectiveness and durability of protective treatments on ceramic materials. Silicon-based coatings, especially nanostructured and functionalized silica gel, followed by alkylpolysiloxane emulsion, have been shown to be the most suitable coatings for outdoor terracotta artefacts, while the fluorinated coating did not provide adequate protection as it was not able to limit water absorption under runoff conditions.

© 2024 The Authors. Published by Elsevier Masson SAS on behalf of Consiglio Nazionale delle Ricerche (CNR).

This is an open access article under the CC BY license (<http://creativecommons.org/licenses/by/4.0/>)

**Abbreviations:** RH, Relative Humidity; T, Temperature; PIM, Mercury Intrusion Porosimetry; XRPD, X-Ray Powder Diffraction; m-RS, Raman micro-Spectroscopy; ESEM, Environmental variable pressure Electron Scanning Microscopy; AAS, Atomic Absorption Spectroscopy; PVDF-HFP, vinylidene fluoride-hexafluoropropylene copolymer; PSw, aqueous emulsion of alkyl polysiloxane; n-SiOR, aqueous dispersion of silica nanoparticles functionalized with short siloxane chains; wnf-SiO<sub>2</sub>, hydroalcoholic solution of silica nanostructured and functionalized with organically modified silicon alkoxides; mv, dry mass variation; C<sub>w</sub>, water absorption capacity; E<sub>Ca</sub>, efficiency of the treatments in reducing Ca release.

\* Corresponding author.

E-mail addresses: [cristina.chiavari@unibo.it](mailto:cristina.chiavari@unibo.it) (C. Chiavari), [elena.bernardi@unibo.it](mailto:elena.bernardi@unibo.it) (E. Bernardi).

<https://doi.org/10.1016/j.culher.2024.09.008>

1296-2074/© 2024 The Authors. Published by Elsevier Masson SAS on behalf of Consiglio Nazionale delle Ricerche (CNR). This is an open access article under the CC BY license (<http://creativecommons.org/licenses/by/4.0/>)

## 1. Introduction

All cultural assets are endangered by the environmental threats linked to the places in which they are located. The deterioration process, whether physical, chemical or biological, is triggered by physical causes, such as water in liquid or vapor phase, from the environment to the object and vice versa [1]. And, what is more, outdoor historical-artistic heritage is increasingly exposed to risks related to climate change and air pollution, which contribute to further accelerate the phenomena of deterioration [2].

Among the different types of ceramics, terracotta is most susceptible to atmospheric agents because of its medium porosity, which determines a strong interaction with the surrounding en-

vironment. Thus, one of the main problems of terracotta is related to the penetration of water and salts dissolved in it through the pores. This phenomenon makes it extremely susceptible to mechanical alterations due to freeze-thaw cycles and crystallization of salts [3,4].

Rain can also play a decisive role from both a mechanical (i.e. erosion) and a chemical point of view. In fact, it can convey acidic and aggressive atmospheric compounds (e.g. SO<sub>x</sub>, NO<sub>x</sub> and CO<sub>2</sub>) to the surfaces, which undergo chemical dissolution [5].

Unfortunately, when taking into account outdoor cultural heritage, it is not possible to control or modify microclimate parameters to suit its proper conservation, as, instead, is the case for indoor collections [6,7]. Hence, an appropriate strategy may consist in direct intervention on the artwork, by interposing a 'barrier' - such as a protective coating- which mitigates the effect of atmospheric agents. By reducing porosity and in turn water absorption, it is possible to reduce spalling and leakage of the ceramic material caused by water expansion as a result of reaching the freezing point[3]. The application of water repellent products, such as Silo 111, can also hinder the absorption of saline solution, thus limiting the crystallization of salts; however, the application of these products may reduce pore interconnection and drying speed [8]. Other studies found out that ethyl silicate coatings were able to reduce the total porosity and enhance water absorption properties as well as durability against acid rains [9,10]. The use of silica or titanium dioxide nanoparticles, integrated or not in polymers, also seem to improve consolidation and hydrophobic properties of ceramic surfaces [11–13].

However, while natural stones have been extensively examined, in the field of conservation, in terms of protection strategies [14–20], few studies have been carried out on consolidants and protective coatings for ceramics [8–13,21]. Out of these few, only part of them concern the performance of commercial products after some form of ageing (e.g. salt crystallization test; distilled water, HCl or H<sub>2</sub>SO<sub>4</sub> solution dripping; irradiation with  $\lambda = 200\text{--}700\text{ nm}$  at constant temperature and relative humidity) [8,10,21].

Most of the protective treatments produced by specialized companies are formulated for general classes of materials rather than specific types; it is therefore extremely important to implement ageing procedures that allow to verify the behavior of the protective treatments before they are actually applied to this kind of material.

The restoration of the contemporary terracotta sculpture "Muro del vento" (Wind Wall) by Domenico Matteucci (Fig. S1 in Supplementary Material), which is part of the Open-Air Museum of Faenza, has been the starting point of this investigation, as it represents an outdoor immovable monumental sculpture that requires an in-depth analysis of the mechanisms responsible for its deterioration and the development of adequate strategies for its proper conservation.

## 2. Research aim

The aims of this research were: (i) to define an artificial ageing and analysis protocol suitable for testing protective treatments for outdoor ceramic materials; (ii) to evaluate the most effective and durable protective coating for terracotta substrates among four different commercial products reported as able to slow down artificial stone deterioration and, to our knowledge, not yet tested on ceramics.

Two different exposure conditions were simulated (acid rain runoff and daily variations of temperature, relative humidity and UVA irradiation) and a long-term outdoor ageing was put in place.

The suitability of the protocol was demonstrated and the effectiveness of the treatments was evaluated through a multi-

analytical approach including surface and chemical-physical analyses.

## 3. Materials and methods

### 3.1. Terracotta specimens

The selected type of clay employed for the production of representative substrates matched that of the "Wind Wall". The artwork in question has a medium porosity (open total porosity ~34 %) and its chemical composition had been previously investigated [22]. Plasma emission spectrophotometry analysis (Tab. S1) highlighted that the artist used a calcium-rich terracotta, obtained through the firing of a clay rich in calcium carbonate. An analogous modern mixture was then selected for producing the specimens: the MB02 mixture by Sila company (Tab. S1). This clay is used by contemporary ceramists for the shaping of large sculptures set for outdoor display. In order to reproduce a real-world scenario, it was decided to replicate also the molding and the firing technique, with the aim of obtaining a similar result to the original one in terms of porosity and defects -which strongly influence the degradation phenomena-. First, two gypsum molds were created for the serial reproduction of the specimens, starting from the modelling of clay positives of the sizes required by the ageing procedures and taking into account the shrinkage during the drying phase. Second, the specimens were fired at a temperature of 980 °C [23] (Fig. S2). Specimens for artificial and outdoor ageing had a final dimension of 5 × 2.5 × 0.5/0.7 cm and of 11.5 × 7 × 1 cm, respectively.

### 3.2. Protective coatings

The selection of the protective coatings was performed according to the following basic criteria [24]: transparency; long-term stability to atmospheric agents and UV radiation; compatibility with the substrate; good hydrophobicity and breathability; no formation of harmful by-products; low toxicity; reversibility and/or re-treatability; ease of application on large surfaces. Four commercial products made for both natural and artificial stone substrates with different chemical compositions were selected (Table 1): i) IDROFLUORO 3® produced by An.t.a.res srl, a vinylidene fluoride-hexafluoropropylene copolymer at 3 % in acetone (PVDF-HFP); ii) IDROSIL ACQUA® produced by An.t.a.res srl, an aqueous emulsion of alkyl polysiloxane (PS<sub>w</sub>), iii) NANO SILO W® produced by CTS srl, an aqueous dispersion of silica nanoparticles functionalized with short siloxane chains (n-SiOR), iv) SiOX-REIOS® produced by Siltea srl, a 10 % hydroalcoholic solution of silica nanostructured and functionalized with organically modified silicon alkoxides (wnf-SiO<sub>2</sub>). Hereafter, the products will be identified by the abbreviation reported in brackets.

All the products were applied by brush over the entire surface of the terracotta specimens (one application), in compliance with the recommendation and the volume/surface ratio reported in the products' technical sheets (about 0.5 l/m<sup>2</sup> for PVDF-HFP and 0.2 l/m<sup>2</sup> for the other products).

### 3.3. Ageing tests

Two different ageing tests were set-up to simulate different exposure conditions and distinctly highlight the effects of acid rain runoff (runoff test) and of the cyclical variation of temperature (T), relative humidity (RH) and UVA radiation (exposure in climate chamber).

The *runoff test* consisted in simulating the mechanical and chemical leaching effect of rain runoff in unsheltered conditions through the dripping of acid rain solution directly on the specimen surface. The composition of the synthetic rain was determined

**Table 1**  
Coatings selected for the research with nominal characteristics provided by suppliers.

Coating	Hydrophobicity/Breathability	Response time	Stability	Compatibility/ Reversibility, re-treatability
PVDF-HFP	It does not alter the permeability to water vapor, water repellent	24 h at 20 °C, protected from direct atmospheric agents	Stable to heat and UV radiation	Reversible in mild organic solvents
PS <sub>w</sub>	It does not alter the permeability to water vapor, water repellent	48 h at 20 °C, protected from rain	Not specified	Compatible with silicate and carbonate matrix stone materials
n-SIOR	Excellent permeability to water vapor, water repellent	24 h at 20 °C, protected from rain	UV resistance	Compatible with silicate and carbonate matrix artificial stone materials, concrete, cement mortars
wnf-SiO <sub>2</sub>	Excellent permeability to water vapor, water repellent	72 h at 20 °C	Not specified	Compatible with terracotta and cementitious materials, reversible with alkaline solution packs

in previous studies to reproduce the characteristics of natural acid rains both in terms of pH (~4.3) and concentration of the main organic and inorganic ions [25]. The test was conducted on three replicates of specimens with each protective treatment, together with three uncoated reference specimens.

All specimens were subjected to the following weekly cycle, used in previous studies for metallic materials [26,27]: two days of rain dripping followed by a one-day break, then three days of dripping and another one-day break. The two weekly stops (drying phase) serve the purpose of allowing a potential recrystallization of material on the surface or within the samples. The specimens were inserted in Teflon sample holders and inclined at 45°. On each specimen, runoff was reproduced thanks to a system of 4 capillary tubes that drop the synthetic rain on the highest front of the specimen surface from a height of about 3 cm and with a total flow of  $54 \pm 1$  ml/h (the experimental device is shown in Fig. S3). At the base of each sample holder, a drainage system collected the rain falling on the samples into a collection tank. After each runoff period, the volume and pH of the collected rain were measured, then a rain sample was acidified by HNO<sub>3</sub> 65 % suprapur and stored at 4 °C in a HDPE bottle for the subsequent calcium analysis. Calcium ion was chosen as a marker element for ceramic dissolution/erosion by the rain, as well as for the efficacy of the coating in preventing these phenomena, since the terracotta used for casting the specimens was carbonate. Moreover, at the end of each runoff period and during the drying phase, the specimens were periodically weighed, until reaching a constant value, in order to evaluate the tendency to release water absorbed during runoff. The test was conducted for a total of 4 weeks, corresponding to 20 days of runoff.

The exposure in climatic chamber (Climacell 111 MMM equipped with Blacklight blue UVA lamps (300–400 nm)) allowed to investigate the reaction of treated and untreated specimens to cyclic variations of temperature, relative humidity and UVA irradiation. Ageing cycles were set-up in order to simulate outdoor daily cycles and to expose the specimens to repeated stress.

Each cycle corresponds to 12 h of exposure (Fig. S4). During the cycle T and RH vary from a cold and humid "night" condition ( $T_{\min}$  5 °C and  $RH_{\max}$  95 %) to a hot and dry "daytime" condition ( $T_{\max}$  65 °C and  $RH_{\min}$  27 %).  $T_{\max}$  value was selected from heat measurements on a terracotta surface exposed to the sun in summer and from experimentation conducted in a previous study [28]. UVA irradiation is set at a power of 4 mW/cm<sup>2</sup>, representative of the average midday irradiance on a clear day in southern European regions. The lamp was on for six hours in "daytime" conditions and off for six hours in "night" conditions.

Three replicates for each protective product, together with three uncoated reference specimens, were exposed, according to ASTM G151–19 [29]. To highlight the possible contribution of UVA irradiation to the ageing, one replica of each type was half covered with tinfoil, leaving it slightly raised to allow air circulation. The

exposure was conducted for a total of 18 days, corresponding to 36 aging cycles.

For both tests, dry weights of the specimens were measured before ( $w_i$ ) and after ageing ( $w_f$ ) (kiln drying at 100 °C until constant mass was reached) and the percentage mass variation ( $mv\%$ ) was calculated as follows:

$$mv\% = [(w_f - w_i)/w_i] \times 100$$

Simultaneously, long-term outdoor ageing was put in place by exposing an additional set of 15 ceramic samples (three uncoated reference and twelve coated specimens) in an open-air terrace of the Museo Internazionale delle Ceramiche in Faenza (Fig. S5). The specimens were placed at a 45° angle, facing south according to ASTM G7/G7M-21 [30]. The thermo-hygrometric values were constantly monitored by a datalogger placed in close proximity, to track environmental conditions. Color measurements were performed after 3 years of field exposure. During this period, T varied between a minimum of –2 °C and a maximum of 51 °C, while RH between a minimum of 17 % and a maximum of 100 %.

### 3.4. Characterization

Uncoated and coated specimens, before and after ageing, were characterized with several techniques to investigate porosity, composition, morphology, color, hydrophobicity and water absorption. Calcium released during runoff test was also determined.

Qualitative mineralogical analyses were performed on powdered samples by X-Ray Powder Diffraction (XRPD) using a Bruker D8 Advance X-Ray diffractometer equipped with LynxEye detector (4–64 2theta, scan velocity 1°/min, and acquisition time = 0.020° step).

Total open porosity and pore size distribution were determined by Mercury Intrusion Porosimetry (PIM) through Thermo Scientific's Pascal 140 and Pascal 240 mercury intrusion porosimeters.

Raman micro-spectroscopy (m-RS) was used for chemical characterization of the specimen surfaces. To acquire reference spectra for the protective products, they were applied to a glass slide. The employed system was a Renishaw Raman InVia spectrometer configured with a Leica DMLM microscope and an Ar<sup>+</sup> laser (514.5 nm,  $P_{\max}$  = 30 mW), as exciting source. In order to avoid sample deterioration and optimize S/N ratio, spectra were acquired by collecting 4 scans (10 s per scan) and reducing the output power at 1.5 mW. After collection, spectra were processed with baseline subtraction by Renishaw WiRE 2.0 software. The characterization of the collected Raman spectra was performed employing Raman spectral databases, such as RRUFF (<https://rruff.info>), expect for cases not expressly indicated in the bibliography.

3D digital surface images were acquired by a HIROX RH-2000 digital microscope (magnification in the 35–5000x range), equipped with a motorized sample holder table that allows an

automatic surface topographic reconstruction (XY movement with micrometric precision (0.04  $\mu\text{m}$ ) for a  $40 \times 40$  displacement).

An environmental variable pressure electron scanning microscope ESEM<sup>TM</sup> Quanta 200, FEI (THERMO FISHER SCIENTIFIC Inc.) was used to observe the specimens also in cross section. The applied working conditions were: Low Vacuum ( $P < 1.5$  Torr), no metallization of the specimens, working distance around 10 mm and HV = 15 kV.

Color measurements were carried out following the UNI EN 15886 standard [31]. The data was collected according to the CIE Lab colour system, where  $a^*$  represents the red/green coordinate,  $b^*$  the yellow/blue one and  $L^*$  Lightness, ranging from 0 (black) to 100 (white). The total color variation due to the application of protective treatments and accelerated ageing was calculated as  $\Delta E^* = (\Delta L^{*2} + \Delta a^{*2} + \Delta b^{*2})^{1/2}$ . According to the guidelines for natural and artificial stone conservation, chromatic alterations due to the applied treatments can be considered not significant when  $\Delta E^* < 3$ , and acceptable when  $\Delta E^* \leq 5$  [32]. Color measurements before and after the treatments were performed with MiniScan EX Plus (HunterLab) in Daylight Color mode (Illuminant/Observer: D65/10°; Geometry: 45–0). The analyses before and after ageing, instead, were carried out by the Datacolor D500 instrument with the following parameters: Illuminant/Observer: D65/10°, Geometry: d/0, Specularity: SCE, Measurement area: 9 mm. On each specimen, measurements were collected at least in three different points.

Water contact angle was measured by Drop Shape Analyzer DSA 30S (Krüss GmbH), which can assess the contact angle of sessile drops on a surface, calculated as the angle between the baseline and the tangent to the fitted drop profile in the liquid-solid-air triple contact point. Measurements were performed after 5 and 60 s from the drop deposition.

Water absorption capacity was evaluated according to the UNI 11085:2003 standard [33]. Specimens dried as described in Section 3.3 were placed on their backs at the bottom of a container and submerged with deionized water for 2.5 h, then weighed again. Percentage water absorption capacity ( $C_w\%$ ) was calculated as follows:

$$C_w\% = [(M_d - M_w)/M_d] \times 100$$

where  $M_d$  represents the mass of the dried specimens and  $M_w$  the mass of the wet specimens.

Calcium released from the specimens during runoff was analyzed by Flame Atomic Absorption Spectroscopy using an AAnalyst 400 AA Spectrometer (PerkinElmer). The absorption was measured

at a wavelength of 422.7 nm; La 0.1 % was added to standards and samples to limit ionization interference. The limit of quantification was 0.1 mg/L: no samples showed concentrations below this limit. Ca was chosen as the reference element since the samples were cast from a carbonate, calcium-rich slurry. The amount of Ca released by each specimen was normalized with respect to its initial dry weight. The efficiency of the treatments in reducing Ca release ( $E_{Ca}$ ) was calculated as:

$$E_{Ca} = \frac{Ca_{UC} - Ca_C}{Ca_{UC}} \times 100$$

where: Ca is the amount of Calcium cumulatively released in the rain at the end of the ageing period; the subscription UC refers to the uncoated specimens and C to the coated ones.  $E_{Ca}$  is 100 if no Ca is released from the coated specimens and 0 % if the coated specimens release as Ca as the uncoated ones.

## 4. Results and discussion

### 4.1. Characterization of terracotta substrates

Unaged uncoated specimens have an orange-brown coloration, typical of terracotta ( $L^* = 58 \pm 2$ ,  $a^* = 19 \pm 1$ ,  $b^* = 28 \pm 2$ ) and a geometric bulk density [34] of  $2.2 \pm 0.4$  g/cm<sup>3</sup>. They are characterized by a unimodal pore size distribution, a rather narrow spectrum in the range 0.1–1  $\mu\text{m}$ . The predominant grain size class is in the range 0.6–0.7  $\mu\text{m}$ , while total open porosity is approximately 30 %, typical of a medium-porous ceramic without coating.

The mineralogical composition, analyzed by XRPD, is typical of ceramic materials obtained using a clay raw material rich in calcium oxide (so-called “carbonate clay”) and fired at a temperature of about 950 °C. This is confirmed by the presence of newly formed minerals, such as gehlenite and pyroxene. Clearly visible are the peaks of quartz, feldspar, hematite and illite (Fig. 1).

Raman micro-spectroscopy, which proved to be a useful technique also for characterizing ceramic materials [35], was performed on several points on the surface of the terracotta substrates, showing the presence of quartz (464 cm<sup>-1</sup>) and silicoaluminates (recognizable feldspathic and plagioclase-type structures, with characteristic bands at 290, 480 and 508–513 cm<sup>-1</sup> [36,37]), as well as titanium dioxide in the form of anatase (main peak at 143 cm<sup>-1</sup> [38]). In addition, iron oxides were identified in form of hematite (well-defined Raman peaks at 225, 247, 295, 410, 500, 610 and 1325 cm<sup>-1</sup>), magnetite (Raman bands at 300, 530 and 660 cm<sup>-1</sup>) and maghemite (wider Raman bands at 350, 500 and 700–720 cm<sup>-1</sup>) [39]. The presence of Mn-based compounds

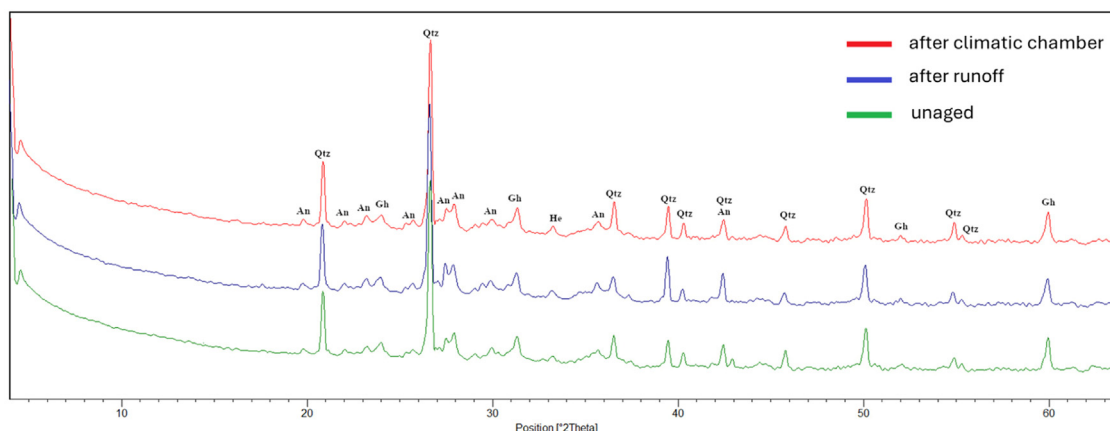


Fig. 1. XRPD spectra of representative terracotta uncoated specimens: unaged, aged by runoff and aged by climatic chamber. (An) Anortite; (Qtz) Quartz; (Gh) Gehlenite; (He) Hematite.

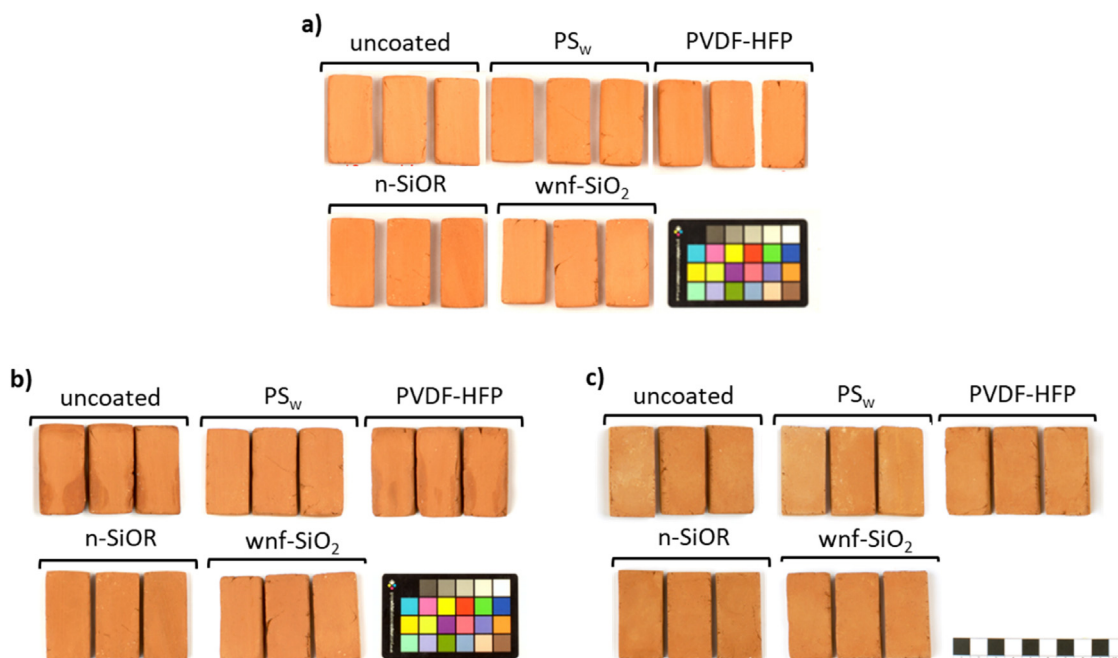


Fig. 2. Images of uncoated and coated specimens (a), specimens aged by runoff test (b) and in climatic chamber (c).

like braunite ( $\text{Mn}^{2+}$ ,  $\text{Mn}^{3+}\text{SiO}_2$ ) was also detected (Fig. S6). Calcium carbonates in the form of calcite and dolomite were distinguished, thanks to the shift of the main band of the symmetric stretching of the carbonate from  $1088$  to  $1098\text{ cm}^{-1}$  [40,41]. Additionally, calcium sulphate (anhydrite) spectrum was detected in its entirety: both the main band of the symmetric stretching of the sulphate group at  $1018\text{ cm}^{-1}$  and the minor bands are clearly visible [42].

The presence of some mineral phases identified by m-RS, such as magnetite, maghemite and braunite, which seem to not be in line with the general oxidizing firing conditions, can be ascribed to impurities in the ceramic raw materials and to local redox conditions [35].

Concerning the mineral phases of carbonate (calcite and dolomite) and the sulphate phase (anhydrite), they can be relict traces of primary mineral phases that were not completely destroyed during the firing process. Specifically, the presence of anhydrite could result from the dehydration of the gypsum due to contamination during the specimens molding (gypsum is the main component of the molds used). In fact, unlike other cases [43], the results of the bulk characterizations here lead to the exclusion of the presence of gypsum in raw materials.

#### 4.2. Characterization of coated terracotta

Concerning the color variations induced by the application of the coatings, n-SiOR caused the starkest change, also visible with the naked eye (Fig. 2a);  $\Delta E^*$  is in fact close to the acceptable threshold of 5 and the variation is mainly related to a decrease in lightness ( $\Delta E^*=5 \pm 1$ , with a  $\Delta L$  of  $-5 \pm 2$ ) (Table 2). PVDF-HFP induced an average  $\Delta E^*$  of  $3 \pm 1$ , not visually detectable. PS<sub>w</sub> and wnf-SiO<sub>2</sub> were the treatments which altered the substrates aspect the less ( $\Delta E^*=2 \pm 1$ ) and therefore turned out to be fully in agreement with the cultural heritage requirement concerning visual properties.

As shown by the images acquired by 3D digital microscope (Fig. S7a), it seems that the application of the protective films causes a variation in the surface microstructure. In fact, the coarse grains clearly visible on uncoated specimens seem to have reduced or dis-

appeared. This also suggests a quite homogeneous coverage by the products.

In order to acquire reference spectra for the m-RS characterization, Raman analyses were preliminary performed on the coatings applied to a glass slide. PS<sub>w</sub>, n-SiOR and wnf-SiO<sub>2</sub> gave rise to a good Raman spectrum, whereas PVDF-HFP to a weaker and noisy spectrum (spectra n.1 in Fig. 3). For all products, the main bands are those relating to the symmetric and asymmetric stretching of the CH bonds, in the range  $2860$ – $2970\text{ cm}^{-1}$ . The different position and intensity of the CH stretching bands allowed characterizing the four as it follows: PVDF-HFP had peaks at  $2895$  and  $2977\text{ cm}^{-1}$ , PS<sub>w</sub> had very strong peaks at  $2906$  and  $2966\text{ cm}^{-1}$ , n-SiOR had two peaks at  $2901$  and  $2962\text{ cm}^{-1}$  and a shoulder at  $2850\text{ cm}^{-1}$ , and wnf-SiO<sub>2</sub> was more structured, with two more intense peak at  $2890$  and  $2931\text{ cm}^{-1}$  and two shoulders at  $2860$  and  $2972\text{ cm}^{-1}$ . Deformation modes of the CH<sub>2</sub>, CH<sub>3</sub> groups were also visible, bringing about weaker bands in the range  $1300$ – $1450\text{ cm}^{-1}$ . On terracotta specimen, the coatings were revealed using CH stretching peaks as markers, as they give the most intense and variously structured Raman bands for the different coatings (spectra n.2 in Fig. 3). In general, the products appear well dispersed, and minerals identified on uncoated specimens (e.g. iron oxides, silicates, anhydrite and calcite) are still detectable.

All coatings, as applied, increase the hydrophobicity of the terracotta specimens, as shown by contact angle measurements (Table 3). In fact, on the uncoated specimens the drop was almost instantly absorbed, while, on the coated ones, contact angle after 5 s increased from about  $55^\circ$  to  $>125^\circ$ . However, the hydrophobic effect did not seem strongly effective in the case of PVDF-HFP, as suggested by the 25 % decrease in contact angle from 5 s to 60 s. This did not occur for wnf-SiO<sub>2</sub>, PS<sub>w</sub> and n-SiOR: these coatings induced a remarkable drop repellency without significant differences between contact angles after 5 s or after 60 s.

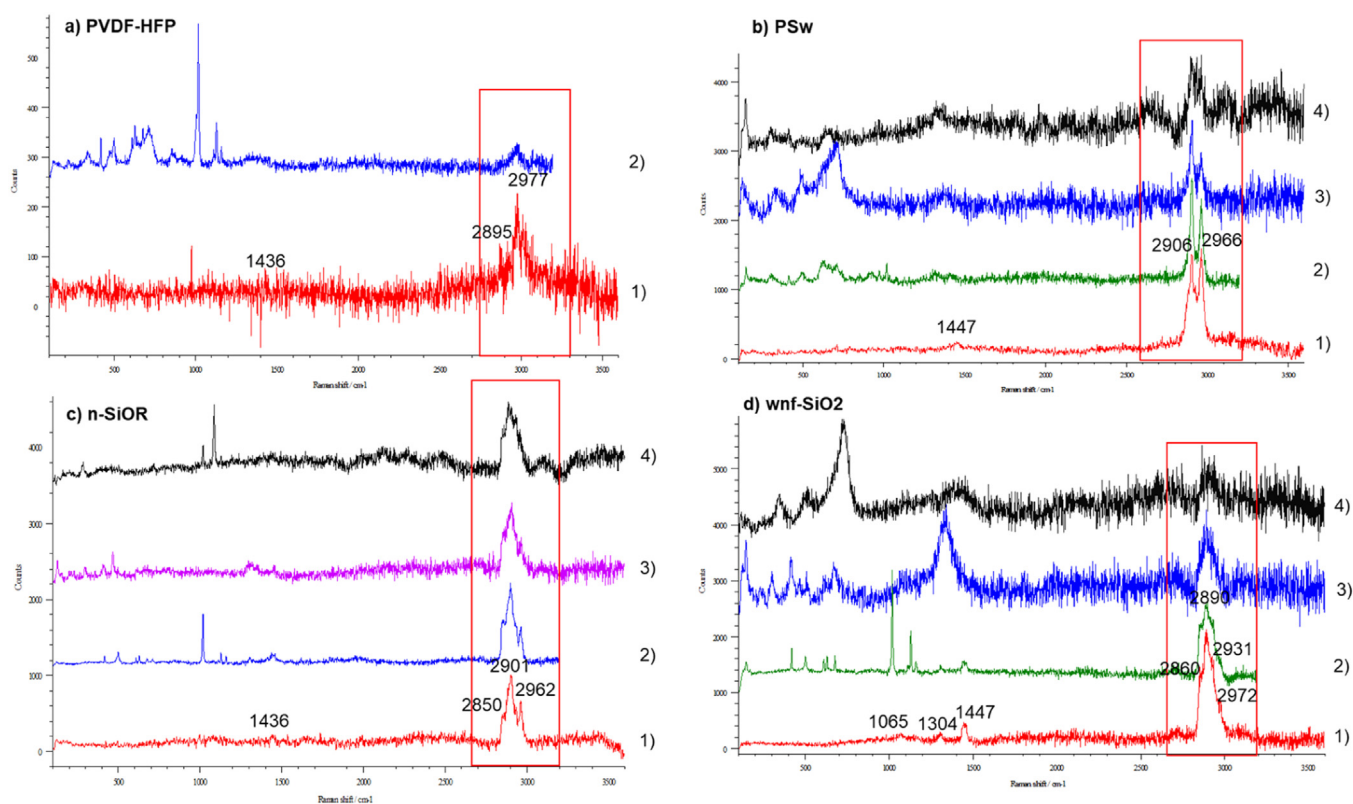
#### 4.3. Accelerated ageing

The mineralogical composition of the terracotta under study seems susceptible to weathering as well as any ceramic material used outdoors. Indeed, it is known that under specific environ-

**Table 2**

Color variations after application of the protective coatings (average of 7 specimens and related standard deviation) and of the uncoated and coated specimens after ageing (average of 3 specimens and related standard deviation). For runoff test, reported data refers to the areas impacted by the rain. Variations detected on covered areas in climatic chamber (1 specimen) are shown in *italic*.

	After Application				After Runoff				After Climatic Chamber			
	$\Delta L^*$	$\Delta a^*$	$\Delta b^*$	$\Delta E^*$	$\Delta L^*$	$\Delta a^*$	$\Delta b^*$	$\Delta E^*$	$\Delta L^*$	$\Delta a^*$	$\Delta b^*$	$\Delta E^*$
<b>Uncoated</b>	–	–	–	–	$-0.4 \pm 0.1$	$0.9 \pm 0.4$	$1.7 \pm 0.5$	$2.0 \pm 0.6$	$0.0 \pm 0.6$	$0.3 \pm 0.4$	$0.1 \pm 0.2$	$0.6 \pm 0.3$
<b>PVDF-HFP</b>	$-2.2 \pm 0.6$	$1.7 \pm 0.9$	$0.8 \pm 0.8$	$3 \pm 1$	$0.0 \pm 0.2$	$0.4 \pm 0.2$	$0.8 \pm 0.6$	$0.9 \pm 0.6$	<i>0.1</i>	<i>-0.1</i>	<i>-0.2</i>	<i>0.3</i>
<b>PS<sub>w</sub></b>	$-0.3 \pm 0.5$	$0.4 \pm 1.3$	$0.6 \pm 1.6$	$2 \pm 1$	$-0.1 \pm 0.1$	$0.1 \pm 0.2$	$-0.7 \pm 0.4$	$0.8 \pm 0.3$	$-0.1 \pm 0.3$	$0.1 \pm 0.2$	$0.2 \pm 0.1$	$0.4 \pm 0.1$
<b>n-SIOR</b>	$-5 \pm 2$	$1.8 \pm 0.6$	$0.6 \pm 0.8$	$5 \pm 1$	$-0.5 \pm 0.1$	$0.3 \pm 0.8$	$0.8 \pm 0.8$	$1.3 \pm 0.4$	<i>-0.4</i>	<i>0.1</i>	<i>-0.4</i>	<i>0.6</i>
<b>wnf-SiO<sub>2</sub></b>	$-1.1 \pm 0.8$	$0.8 \pm 0.5$	$-0.2 \pm 0.4$	$2 \pm 1$	$-0.2 \pm 0.3$	$0.4 \pm 0.2$	$0.4 \pm 0.3$	$0.6 \pm 0.4$	$0.9 \pm 1$	$-0.5 \pm 0.6$	$-0.7 \pm 0.6$	$1.4 \pm 1.0$
									<i>-1.4</i>	<i>1.0</i>	<i>0.2</i>	<i>1.8</i>
									$1.9 \pm 0.7$	$-0.6 \pm 0.2$	$0.0 \pm 0.7$	$2.1 \pm 0.5$
									$1.8$	$-0.7$	$0.0$	$2.0$
									$-0.3 \pm 0.5$	$0.1 \pm 0.1$	$0.1 \pm 0.3$	$0.5 \pm 0.1$
									<i>-0.3</i>	<i>-0.3</i>	<i>-0.0</i>	<i>0.4</i>



**Fig. 3.** Raman spectra of the coatings in different conditions. Coatings: A) PVDF-HFP; B) PS<sub>w</sub>; C) n-SIOR; D) wnf-SiO<sub>2</sub>. Conditions: 1) fresh coating on mirror glass; 2) fresh coated terracotta; 3) runoff aged coated terracotta; 4) climatic chamber aged coated terracotta.

mental conditions, such as prolonged contact with water or high humidity, gehlenite can turn into wairakite and calcite [44], causing, in the long term, even the physical degradation of the ceramic product. This mineralogical transformation, however, did not occur under the applied ageing conditions: both the ageing by runoff and in the climatic chamber, in fact, do not seem to have caused changes in the mineralogy, as highlighted by XRPD spectra (Fig. 1). Raman spectra locally recorded on uncoated specimens continued to detect calcite, quartz and silicates, and iron oxides (especially haematite); on specimens aged in climatic chamber also anatase and rutile (main bands at 445 and 610 cm<sup>-1</sup> [45], spectrum not shown) were identified.

After climatic chamber ageing, the aspect of both the uncoated and coated specimens was not significantly altered at a microscopic level (crf. Fig. S7a vs. c and Fig. S8a vs. c). In contrast, after runoff ageing, streaks were visible under the 3D digital microscope on both uncoated and coated specimens (Fig. S7b). In addition, op-


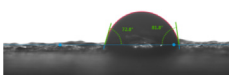
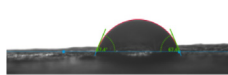
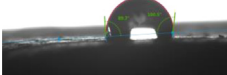
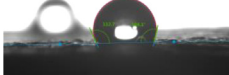
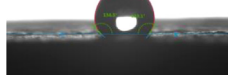
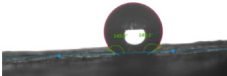
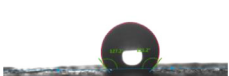
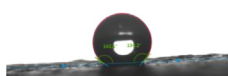
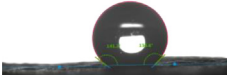

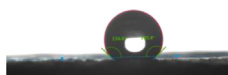
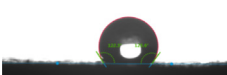

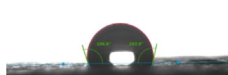
tical microscope observation revealed the formation of pores in the areas that were directly impacted by the rain flow (crf. Fig. S8b1 vs. b2), especially on the uncoated specimens where pores are more numerous and tend to be wider (diameter  $\geq 40 \mu\text{m}$ ). This effect is ascribable to the mechanical/chemical action of the rain runoff which, albeit to a less extent, also affected the coated specimens.

Nevertheless, ESEM observations carried out in cross section confirm the presence of coatings on the aged surfaces (Fig. S9), even if they do not allow to clarify whether the protective films remain continuously on the entire surface.

Additionally, Raman analyses, performed on several points on the surfaces, showed that PS<sub>w</sub> (Fig. 3b), n-SIOR (Fig. 3c) and wnf-SiO<sub>2</sub> (Fig. 3d) were still present after ageing under both conditions and, in the case of wnf-SiO<sub>2</sub>, spectra tended to be less evident after climatic chamber than after runoff. Only PVDF-HFP was no longer detected by Raman, neither after runoff nor after climatic chamber ageing. Specimens coated with the fluorinated product determined

**Table 3**

Contact angles measured after 5 s ( $t_0$  5 s) and after 60 s ( $t_f$  60 s) on uncoated and coated specimens, unaged and after ageing (runoff and climatic chamber). Average and standard deviations of at least 3 measurements in different areas are reported. Representative images of the drops at  $t_f$  60 s are shown, except for uncoated specimens for which drops at  $t_0$  5 s are shown.

	Unaged			After Runoff			After Climate Chamber		
	$t_0$ 5s	$t_f$ 60s	Image	$t_0$ 5s	$t_f$ 60s	Image	$t_0$ 5s	$t_f$ 60s	Image
Uncoated	54 ±8	0 <sup>(°)</sup>		78 ±4	0 <sup>(*)</sup>		72 ±5	0 <sup>(#)</sup>	
PVDF-HFP	128 ±5	96 ±8		125 ±3	112 ±6		136 ±3	129.2 ±0.6	
PS <sub>w</sub>	145 ±7	144 ±5		130.4 ±0.1	129.1 ±0.2		135 ±2	135 ±1	
n-SiOR	144 ±2	142 ±4		135.7 ±0.1	135.7 ±0.1		136 ±2	134 ±1	
wnf-SiO <sub>2</sub>	126 ±3	122 ±4		114 ±3	101 ±7		113.8 ±0.8	104 ±1	

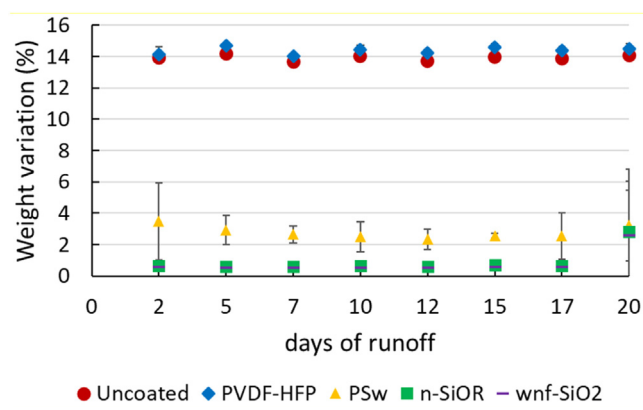
(°) $t_f$  5 s; (\*) $t_f$  8 s; (#) $t_f$  30 s

a high level of fluorescence that covered completely the Raman signals - an effect which is likely ascribable to the ageing of the residual polymer on the surface.

This is in agreement with the results of contact angle measurements (Table 3). In fact, after both the ageing tests, all the coated specimens had contact angles ( $t_0$  5 s) from 1.5 to 1.9 times higher than the uncoated ones, and substantially maintained their initial level of hydrophobicity. As regards the absorption rate ( $t_f$  60 s vs.  $t_0$  5 s in Table 3), in the case of uncoated specimens drops continued to be absorbed within a few seconds (from about 8 s after runoff test to about 30 s after climatic chamber): this slightly lower absorption rate with respect to the unaged specimens could be explained by a change in pore size such as to induce a slight retention of the drop. On the contrary, on coated surfaces, contact angles after 60 s remained always higher than 114°. Taking into account the behavior of each single coating, PVDF-HFP confirmed to not be properly effective in preventing water absorption, as also demonstrated by water absorption measurements performed after ageing (Fig. S10). PS<sub>w</sub> and n-SiOR remained very effective under all the ageing conditions -as demonstrated by the non-significant change in contact angle and drop shape between  $t_0$  5 s and  $t_f$  60 s. wnf-SiO<sub>2</sub> showed a slight increase in surface wettability after ageing, thus suggesting that ageing may have slightly affected the stability of the coating.

In any case, according to these results, it seems possible to state that the applied coatings remained quite homogeneously present in the surface layer even after ageing, and that they were not completely removed by the mechanical effect of runoff.

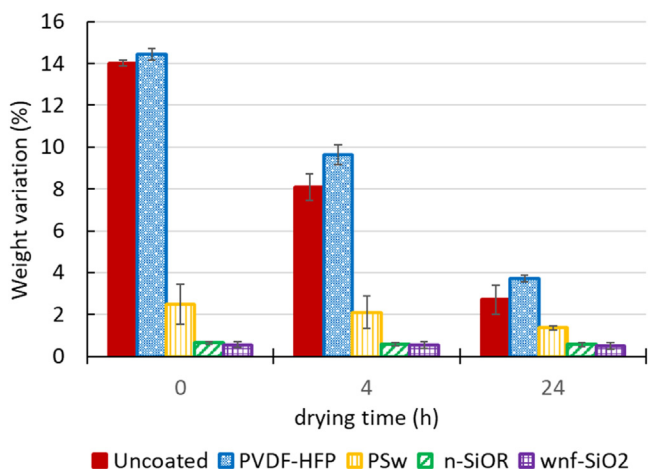
In general, after ageing in climatic chamber (Fig. 2c), all coatings revealed a very good lightfastness both to T/RH cycles and to UVA irradiation, with an average  $\Delta E^*$  always lower than 2, even for uncoated specimens. Specifically, UVA did not seem to have a significant effect on the coatings, in fact  $\Delta E^*$  between covered and uncovered areas is always lower than 1.



**Fig. 4.** Percentage weight variation of the wet specimens at the end of each runoff phase with respect to the initial dry weight (average of three specimens per type and related standard deviation).

After runoff test (Fig. 2b), all coated specimens showed no appreciable color variation, with an average  $\Delta E^*$  always lower than  $1.3 \pm 0.4$ , compared to the uncoated ones ( $\Delta E^* = 2.0 \pm 0.6$ ). However, while the surfaces of the specimens coated with PS<sub>w</sub>, n-SiOR and wnf-SiO<sub>2</sub> were homogeneous (i.e. no differences between the areas reached directly and indirectly by the rain flow), both uncoated and PVDF-HFP specimens resulted visibly darker in the small areas which were not directly reached by the rain flow. In these specific areas the following color variations were recorded:  $\Delta E^* = 5.5 \pm 0.7$  with a  $\Delta L^*$  of  $-4.2 \pm 0.4$  for the uncoated, and  $\Delta E^* = 4.5 \pm 0.5$  with a  $\Delta L^*$  of  $-4.0 \pm 0.5$  for the PVDF-HFP specimens.

This could be due to different water absorption and evaporation rates between the two areas. Indeed, as discussed previously,

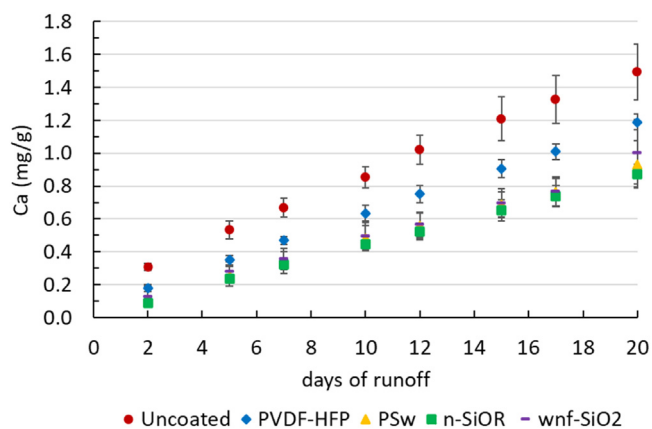


**Fig. 5.** Estimation of the evaporation rate after 10 days of runoff: percentage variation of the specimens' weights at 0, 4 and 24 h after the end of the runoff phase with respect to their dry weights before ageing (average of three specimens per type and related standard deviation).

the uncoated specimens, followed by those coated with PVDF-HFP, showed almost instantaneous or rapid water absorption (Table 3). Therefore, water may have penetrated from runoff areas and then diffused through the specimens. Furthermore, since the formation of pores was observed in the areas of direct rain flow (Fig. S8), it is also possible that, during the drying phase, water evaporated more slowly from the indirectly wetted areas, leaving a darker shadow. This hypothesis is further supported by the disappearance of the shadow after drying at 100 °C for dry weight measurement at the end of ageing.

In the case of runoff test, with the aim of providing further information on water absorption (Fig. 4) and retention (Fig. 5) over time, specimens were weighed at the beginning and during the drying phases. The results were overall in agreement with findings of contact angle measurements.

In fact, from the very first days of ageing, uncoated and PVDF-HFP-coated specimens consistently absorbed a comparable and significantly greater amount of water than PS<sub>w</sub>, n-SiOR and wnf-SiO<sub>2</sub> - coated specimens (Fig. 4). In the case of the latter products, even if the overall differences among them are not statistically significant ( $\alpha = 0.05$ ), it seems that PS<sub>w</sub> tends to absorb slightly more water than n-SiOR and wnf-SiO<sub>2</sub> during the ageing, and that the

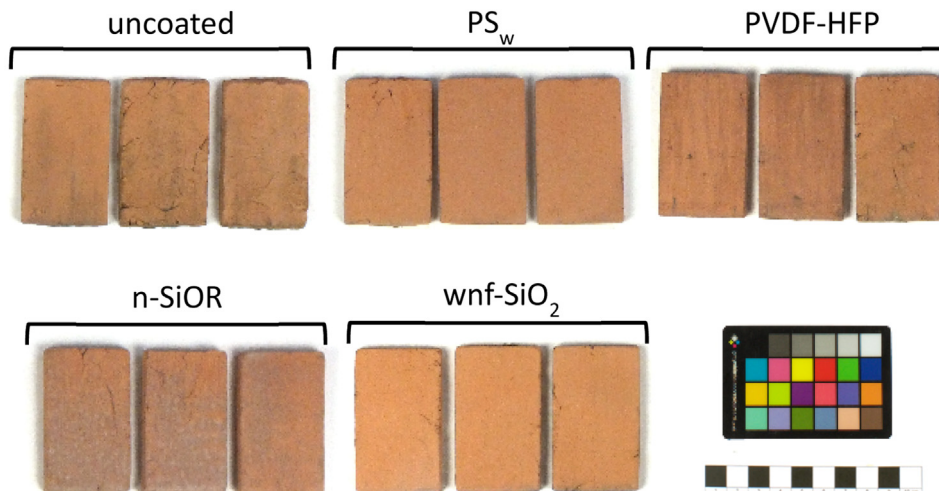


**Fig. 6.** Cumulative calcium release under runoff ageing, in relation to the specimens' initial dry weight (mg/g) and averaged by sample type (average of three specimens per type and related standard deviation).

absorption of n-SiOR and wnf-SiO<sub>2</sub> tends to increase at the end of the ageing, reaching that of PS<sub>w</sub>.

Evaporation rate (estimated by weighing the specimens during the drying phase) showed that uncoated, and especially PVDF-HFP specimens, require more time than the other specimens to stabilize their weight, as expected given their greater water absorption capacity. As a matter of fact, in these cases, the higher amount of water absorbed during runoff continued to evaporate during all the 24 h drying phase (Fig. 5). PS<sub>w</sub>-coated specimens were rather slow in water evaporation, while, for both n-SiOR and wnf-SiO<sub>2</sub>, the low weight variation due to the negligible amount of absorbed water remained constant.

The analyses performed on the rain solution during runoff showed that in general Ca was released with linear increasing trends. In addition, as foreseen, the uncoated specimens cumulatively released more Ca ( $1.5 \pm 0.2$  mg/g) and with a higher release rate than the coated ones (Fig. 6). Among the coatings, in accordance with the previously discussed results, PVDF-HFP demonstrated the lowest efficiency in reducing Ca release ( $E_{Ca}(\text{PVDF-HFP}) = 20 \pm 12\%$ ), while PS<sub>w</sub>, n-SiOR and wnf-SiO<sub>2</sub> displayed similar trends and values. Only at the end of ageing, they seem to be inclined to differ slightly, even if the  $E_{Ca}$  remains comparable and higher than that of PVDF-HFP ( $E_{Ca}(\text{PS}_w) = 38 \pm 15\%$ ;  $E_{Ca}(\text{n-SiOR}) = 42 \pm 13\%$ ;  $E_{Ca}(\text{wnf-SiO}_2) = 33 \pm 18\%$ ).



**Fig. 7.** Images of coated and uncoated terracotta specimens after 3 years of unsheltered outdoor exposure.



Lastly, after both ageing conditions, dry mass variations (Tab. S2) presented a general very slight mass gain ( $\leq 1.6\%$ ), likely ascribable to the formation of salts in the specimens [46]. Specifically, this is noticeable in PVDF-HFP under runoff conditions, as it showcases the highest water absorption and retention (Fig. 5).

#### 4.4. Natural weathering

In addition to the artificial ageing tests previously described, a long-term outdoor ageing was carried out (Section 3.3). After 3 years of exposure, an intermediate evaluation was performed through visual observation (Fig. 7) and color measurements (Tab. S3).

Under natural ageing conditions, which includes others environmental parameters such as particulate matter and biological communities (e.g. bacteria, fungi, algae and mosses), acceptable and not significant color variations have been detected for specimens coated by PS<sub>w</sub> ( $\Delta E^* = 4.3 \pm 0.4$ ) and wnf-SiO<sub>2</sub> ( $\Delta E^* = 2 \pm 1$ ), respectively. Therefore, PS<sub>w</sub> and, primarily, wnf-SiO<sub>2</sub> seem to be able to provide for good protection against aesthetical alterations. The other specimens show a  $\Delta E^*$  well above 5. Specifically, the uncoated terracotta is characterized by lightness decrease, the PVDF-HFP-coated specimens by a lightness decrease together with an increase in the blue component, while n-SiOR-coated ones by an increase in green and blue components. These significant color variations may be due to both soiling (loss of reflectance related to negative  $\Delta L^*$ ) and biological contamination, which especially affects the color shift towards green and blue shades.

## 5. Conclusions

The work in question allowed to define an experimental protocol for the accelerated testing of the effectiveness and durability of protective treatments for ceramic materials, as well as to identify suitable protective coatings for terracotta located outdoors, among those generally recommended for natural and artificial stones, since - to the best of our knowledge - specific products have not yet been developed for this type of material. Specifically, four commercial coatings (one fluorinated copolymer and three silicon based) were tested on terracotta specimens representative of outdoor works of arts. The proposed artificial ageing and analytical protocol was able to simulate and assess the coating behavior under the chemical-physical action of acid rain runoff, thermohygro-metric variations and UVA irradiation, providing a suitable tool for the verification of the effectiveness of protective treatments before being actually applied to terracotta cultural heritage.

These are the overall outcomes:

- The application of the selected coatings, except for n-SiOR, does not cause appreciable color changes in terracotta. In any case, once applied and exposed to the action of acid rain, heat, humidity and UVA rays, all products undergo negligible color variations.
- All coatings decrease the wettability of the terracotta both before and after ageing, proving that they can remain in the surface layer even in spite of the abrasive and chemical effect exerted by rain runoff (noticeable by 3D digital microscope images and Ca release analyses).
- The fluorinated coating, on the basis of Raman analyses, appears to be less stable than the silicon-based products and, although it reduces the wettability of the substrate, it does not sufficiently limit water absorption, even before ageing. Furthermore, under rain exposure, the specimens covered with this coating behave similarly to the uncoated ones, also with regard to the appearance of dark shadows potentially due to differences in the absorption and evaporation rates between areas of the surface with different wetting.

- Silicon-based coatings have a similar behavior to each other and maintain their good hydrophobicity over time, by limiting water penetration also during and after ageing. Among them, PS<sub>w</sub> seems to limit the evaporation of the little absorbed water slightly more.

Observations of the specimens after three years of natural weathering in unsheltered conditions confirm and integrate laboratory findings. As a matter of fact, specimens with the fluorinated coating appear similar to the uncoated ones; PS<sub>w</sub> and, in particular, wnf-SiO<sub>2</sub> provide a good protection, while n-SiOR, which induced a significant color variation already at the application stage, displays a visible surface alteration.

In conclusion, based on these findings and taking into account effectiveness and durability, as well as aesthetic evaluations, the use of PS<sub>w</sub> (aqueous emulsion of alkyl polysiloxane) and especially wnf-SiO<sub>2</sub> (hydroalcoholic solution of silica nanostructured coating functionalized with organically modified silicon alkoxides) seem suitable for application to outdoor terracotta cultural heritage, while the use of vinylidene-fluoride-hexafluoropropene copolymer should be discouraged for this type of substrate.

## CRediT authorship contribution statement

**S. Spadavecchia:** Investigation, Data curation, Formal analysis, Visualization, Writing – original draft, Writing – review & editing. **C. Chiavari:** Conceptualization, Methodology, Writing – original draft, Writing – review & editing, Supervision. **F. Ospitali:** Investigation, Data curation, Visualization, Writing – original draft. **S. Gualtieri:** Investigation, Data curation, Formal analysis, Visualization, Writing – review & editing. **A.C. Hillar:** Writing – review & editing. **E. Bernardi:** Conceptualization, Methodology, Data curation, Formal analysis, Validation, Visualization, Writing – original draft, Writing – review & editing, Supervision.

## Acknowledgements

The Authors would like to acknowledge Dr. Cecilia Velino for her support in performing artificial ageing and to Dr. Valentina Mazzotti for allowing the natural ageing of the samples at the International Ceramics Museum of Faenza.

## Supplementary materials

Supplementary material associated with this article can be found, in the online version, at [doi:10.1016/j.culher.2024.09.008](https://doi.org/10.1016/j.culher.2024.09.008).

## References

- [1] Istituto Centrale del Restauro *Fattori di deterioramento, Parte II, Modulo 1, DI-MOS, Roma, 1979 pp. V-X.*
- [2] Global Climate Change on Built Heritage and Cultural Landscapes The Noa's Ark Project, Atlas and Guidelines, 2007 <https://cordis.europa.eu/project/id/501837/it>.
- [3] B. Fabbri, C. Ravanelli Guidotti, *Il Restauro Della Ceramica*, Nardini Editore, Firenze, 2004, pp. 91–98.
- [4] S. Chatterji, Aspects of generation of destructive crystal growth pressure, *J. Cryst. Growth* 277 (2005) 566–577, doi:10.1016/j.jcrysgro.2004.12.036.
- [5] A. Bonazza, P. Messina, C. Sabbioni, C.M. Grossi, P. Brimblecombe, *Mapping the impact of climate change on surface recession of carbonate buildings in Europe*, *Sci. Total Environ.* 407 (2009) 2039–2050, doi:10.1016/j.scitotenv.2008.10.067.
- [6] D. Camuffo, *Microclimate for Cultural Heritage. Measurement, Risk Assessment, Conservation, Restoration and Maintenance of Indoor and Outdoor Monuments*, 3rd Edition, Elsevier, 2019 ISBN 9780444641069.
- [7] E. Lucchi, Review of preventive conservation in museum buildings, *J. Cult. Herit.* 29 (2018) 180–193, doi:10.1016/j.culher.2017.09.003.
- [8] G. Cultrone, F. Madkour, Evaluation of the effectiveness of treatment products in improving the quality of ceramics used in new and historical buildings, *J. Cult. Herit.* 14 (2003) 304–310, doi:10.1016/j.culher.2012.08.001.

- [9] E. Franzoni, B. Pigino, A. Leeman, P. Lura, Use of TEOS for fired-clay bricks consolidation, *Mater. Struct.* 47 (2013) 1175–1184, doi:10.1617/s11527-013-0120-7.
- [10] V.E. García-Vera, A.J. Tenza-Abril, M. Lanzoñ, The effectiveness of ethyl silicate as consolidating and protective coating to extend the durability of earthen plasters, *Constr. Build. Mater.* 236 (2020) 1–8, doi:10.1016/j.conbuildmat.2019.117445.
- [11] M.G. Mohamed, N.M. Ahmed, W.S. Mohamed, A.H. Ibrahim, H.M. Mohamed, The potential of new eco-friendly formulations in enhancing the protection of ceramic artifacts, *J. Cult. Herit.* 67 (2024) 404–413, doi:10.1016/j.culher.2024.04.003.
- [12] M.M. Ibrahim, S. Omar, Y. Hefni, A.I. Ahmed, Nanomaterials for Consolidation and Protection of Egyptian Faience form Matteria, Egypt, *J. Nano Res.* 56 (2019) 39–48, doi:10.4028/www.scientific.net/JNanoR.56.39.
- [13] M. Barberio, S. Veltri, A. Imbrogno, F. Stranges, A. Bonanno, P. Antici, TiO<sub>2</sub> and SiO<sub>2</sub> nanoparticles film for cultural heritage: conservation and consolidation of ceramic artifacts, *Surf. Coat. Technol.* 271 (2015) 174–180, doi:10.1016/j.surfcoat.2014.12.045.
- [14] G. Graziani, E. Sassoni, G.W. Scherer, E. Franzoni, Resistance to simulated rain of hydroxyapatite- and calcium oxalate- based coatings for protection of marble against corrosion, *Corros. Sci.* 127 (2017) 168–174, doi:10.1016/j.corsci.2017.08.020.
- [15] E. Hansen, E. Doehne, J.A. Fidler, J. Larson, B. Martin, M. Matteini, C. Rodriguez-Navarro, E. Sebastián, C. Price, A. De Tagle, J.M. Teutonico, N. Weiss, A review of selected inorganic consolidants and protective treatments for porous calcareous materials, *Stud. Conserv.* 4 (2003) 13–25. doi:10.1179/sic.2003.48. Supplement-1.13.
- [16] Z. Kaplan, H. Böke, A. Sofuoglu, B. Ipekoglu, Long term stability of biodegradable polymers on building limestone, *Prog. Org. Coat.* 131 (2019) 378–388, doi:10.1016/j.porgcoat.2019.03.004.
- [17] M.K. Khallaf, A.A. El-Mindany, S.E. El-Mofty, Influence of acrylic coatings on the interfacial, physical, and mechanical properties of stone-based monuments, *Prog. Org. Coat.* 72 (2011) 592–598, doi:10.1016/j.porgcoat.2011.06.021.
- [18] P. Maravelaki-Kalaitzaki, N. Kallithrakas-Kontos, D. Korakaki, Z. Agioutantis, S. Maurigiannakis, Evaluation of silicon-based strengthening agents on porous limestones, *Prog. Org. Coat.* 57 (2006), doi:10.1016/j.porgcoat.2006.08.007.
- [19] L. de Ferri, P.P. Lottici, A. Lorenzi, A. Montenero, E. Salvioli-Mariani, Study of silica nanoparticles – polysiloxane hydrophobic treatments for stone-based monument protection, *J. Cult. Herit.* 12 (2011) 356–363, doi:10.1016/j.culher.2011.02.006.
- [20] A. Artesani, F. Di Turo, M. Zucchelli, A. Traviglia, Recent advances in protective coatings for cultural heritage—an overview, *Coatings* 10 (2020) 1–36, doi:10.3390/coatings10030217.
- [21] A.V. Oancea, G. Bodi, A. Cernescu, I. Spiridon, A. Nicolescu, M. Drobot, C. Cotofana, B.C. Simionescu, M. Olaru, Protective coatings for ceramic artefacts exposed to UV ageing, *Npj. Mater. Degrad.* 7 (2023) 21, doi:10.1038/s41529-023-00343-8.
- [22] A.M. Lega, V. Mazzotti, B. Fabbri, D. Pinna, in: *Progetto Di Conservazione Programmata Di Ceramiche Del Novecento Esposte All'aperto Nel Centro Storico Di Faenza, Atti del XX Convegno di Studi (Bressanone 13-16 Luglio, Edizioni Arcadia Ricerche, 2004, pp. 503–512.*
- [23] UNI 10739:1998, *Beni Culturali - Tecnologia ceramica - Termini e definizioni*, Milano, 1998.
- [24] *NORMAL 20/85Materiali lapidei: "Criteri per la progettazione ed il controllo degli interventi conservativi su materiali lapidei"*, CNR-ICR, Roma, 1986.
- [25] E. Bernardi, C. Chiavari, B. Lenza, C. Martini, L. Morselli, F. Ospitali, L. Robbiola, The atmospheric corrosion of quaternary bronzes: the leaching action of acid rain, *Corros. Sci.* 51 (2009) 159–170, doi:10.1016/j.corsci.2008.10.008.
- [26] G. Masi, E. Bernardi, C. Martini, I. Vassura, L. Skrelp, E.S. Fabian, N. Gartner, T. Kosec, C. Josse, J. Esvan, M.C. Bignozzi, L. Robbiola, C. Chiavari, An innovative multi-component fluoropolymer-based coating on outdoor patinated bronze for Cultural Heritage: durability and reversibility, *J. Cult. Herit.* 45 (2020) 122–134, doi:10.1016/j.culher.2020.04.015.
- [27] C. Chiavari, E. Bernardi, A. Balbo, C. Monticelli, S. Raffo, M.C. Bignozzi, C. Martini, Atmospheric corrosion of fire-gilded bronze: corrosion and corrosion protection during accelerated ageing tests, *Corros. Sci.* 100 (2015) 435–447, doi:10.1016/j.corsci.2015.08.013.
- [28] S. Afra, C. Gabbriellini, M. Galeotti, in: *Le opere ceramiche invetriate poste in esterno: problemi conservativi e tecniche di integrazione della lacuna*, Bollettino del Museo Internazionale delle Ceramiche in Faenza 1–2, Edizioni Polistampa, 2019, pp. 67–73.
- [29] ASTM G151–19, *Standard practice for exposing nonmetallic materials in accelerated test devices that use laboratory light sources.*
- [30] ASTM G7/G7M-21, *Standard practice for natural weathering of materials.*
- [31] UNI EN 15886, *Conservazione Dei Beni Culturali – Metodi di Prova – Misura del Colore Delle Superfici*, Milano, 2010.
- [32] J. Delgado Rodrigues, A. Grossi, Indicators and ratings for the compatibility assessment of conservation actions, *J. Cult. Herit.* 8 (2007) 32–43, doi:10.1016/j.culher.2006.04.007.
- [33] UNI 11085:2003, *Beni Culturali - Materiali lapidei Naturali Ed Artificiali - Determinazione del Contenuto d'acqua: Metodo ponderale*, Milano, 2003.
- [34] ISO 18754:2020 *Fine ceramics (advanced ceramics, advanced technical ceramics) - determination of density and apparent porosity.*
- [35] C. Germinario, G. Cultrone, A. De Bonis, F. Izzo, A. Langella, M. Mercurio, L. Nodari, C.R. Vyhnal, C. Grifa,  $\mu$ -Raman spectroscopy as a useful tool for improving knowledge of ancient ceramic manufacturing technologies, *Appl. Clay Sci.* 253 (2024), doi:10.1016/j.clay.2024.107347.
- [36] J.J. Freeman, A. Wang, K.E. Kuelber, B.L. Jolliff, L.A. Haskin, Characterization of natural feldspars by Raman spectroscopy for future planetary exploration, *Canadian Mineral.* 46 (2008) 1477–1500, doi:10.3749/canmin.46.6.1477.
- [37] D. Bersani, I. Aliatis, M. Tribaudino, L. Mantovani, A. Benisek, M.A. Carpenter, G.D. Gatta, P.P. Lottici, Plagioclase composition by Raman spectroscopy, *J. Raman Spectrosc.* 49 (2018) 684–698, doi:10.1002/jrs.5340.
- [38] T. Ohsaka, Temperature dependence of the Raman spectrum in anatase TiO<sub>2</sub>, *J. Phys. Soc. Jpn.* 48 (1980) 1661 [https://ui.adsabs.harvard.edu/link\\_gateway/1980JPSJ...48.1661O](https://ui.adsabs.harvard.edu/link_gateway/1980JPSJ...48.1661O), doi:10.1143/JPSJ.48.1661.
- [39] D.L.A. De Faria, S. Venancio Silva, M.T. de Oliveira, Raman microspectroscopy of some iron oxides and oxyhydroxides, *J. Raman Spectrosc.* 28 (1997) 873–878. doi:10.1002/(SICI)1097-4555(199711)28.11%3C873::AID-JRS177%3E3.0.CO;2-B, doi:10.1002/(SICI)1097-4555(199711)28.
- [40] J. Urmos, S.K. Sharma, F.T. Mackenzie, Characterization of some biogenic carbonates with Raman Spectroscopy, *Am. Mineral.* 76 (1991) 641–646.
- [41] J. Sun, Z. Wu, H. Cheng, Z. Zhang, R.L. Frost, A Raman spectroscopic comparison of calcite and dolomite, *Spectrochim. Acta Part A* 117 (2014) 158–162, doi:10.1016/j.saa.2013.08.014.
- [42] L. Burgio, R.J.H. Clark, Library of FT-Raman spectra of pigments, minerals, pigment media and varnishes, and supplement to existing library of Raman spectra of pigments with visible excitation, *Spectrochim. Acta Part A* 57 (2001) 1491–1521, doi:10.1016/S1386-1425(00)00495-9.
- [43] S. Gualtieri, The glazed tiles of the Thomas Strobl stove: an archaeometric study, *J. Cult. Herit.* 46 (2020) 399–406, doi:10.1016/j.culher.2020.09.017.
- [44] B. Fabbri, S. Gualtieri, S. Shoval, The presence of calcite in archaeological ceramics, *J. Eur. Ceram. Soc.* 34 (7) (2014) 1899–19, doi:10.1016/j.jeurceramsoc.2014.01.007.
- [45] D. Krishnamurti, The Raman spectrum of rutile, *Proc. Indian Acad. Sci.* 55 (1962) 290–299.
- [46] T. Stryzewska, S. Kańska, The effects of salt crystallization in ceramic bricks in terms of line deformation, *Procedia Eng.* 193 (2017) 120–127, doi:10.1016/j.proeng.2017.06.194.